Fusion Engineering and Design 124 (2017) 396–400

Contents lists available at ScienceDirect

Fusion Engineering and Design

journal homepage: www.elsevier.com/locate/fusengdes

Tensile deformation behavior of tungsten fibre-reinforced tungsten composite specimens in as-fabricated state

H. Gietl[a,b,*], J. Riesch[a], J.W. Coenen[c], T. Höschen[a], Ch. Linsmeier[c], R. Neu[a,b]

[a] Max-Planck-Institut für Plasmaphysik, 85748 Garching, Germany
[b] Technische Universität München, lBoltzmannstrasse 15, 85748 Garching, Germany
[c] Forschungszentrum Jülich GmbH, Institut fuer Energie und Klimaforschung, Partner of the Trilateral Euregio Cluster (TEC), 52425 Juelich, Germany

HIGHLIGHTS

- Material qualification of tungsten fibre-reinforced tungsten composite by means of tension tests.
- In the as-fabricated condition samples the material is still able to bear rising load despite multiple matrix cracks.
- Fibre necking as well as fibre pull out was observed leading to the typical pseudo ductile behavior of the composite.
- The description of the mechanical tests will be supplemented by detailed microstructural investigations.

ARTICLE INFO

Article history:
Received 1 October 2016
Received in revised form 8 February 2017
Accepted 14 February 2017
Available online 2 March 2017

Keywords:
Tungsten
Fibre-reinforced composite
Tensile test
Ultimate tensile strength

ABSTRACT

To overcome the inherent brittleness of tungsten, which is a promising candidate for a plasma-facing material in a future fusion device, tungsten fibre-reinforced tungsten composites (W_f/W) have been developed. As a part of the materials characterisation program on W_f/W, we present the results of first tensile tests of as-fabricated W_f/W in this contribution. The results give insight on the ultimate tensile strength properties and reveal the active toughening mechanisms under tension load within the composite. Fibre bridging, fibre necking as well as fibre pull out were observed. This is leading to the typical pseudo ductile behavior of the composite which is characterized by a rising load bearing capability despite multiple matrix cracks accompanied by non catastrophic crack propagation (in the matrix). The description of the mechanical tests is supplemented by detailed microstructural investigations.

1. Introduction

Tungsten is a promising plasma-facing material for future fusion reactors due to its unique property combination such as a low sputter yield, a high melting point and a low activation [1]. The main drawbacks for the use of pure tungsten are its brittleness below the ductile-to-brittle transition temperature [2–4] and the embrittlement during operation e.g. by overheating and/or neutron irradiation [5–7]. These limitations are mitigated by using tungsten fibre-reinforced tungsten composite (W_f/W) which utilizes extrinsic mechanisms to improve the toughness [8–10] similar to ceramic fibre-reinforced ceramics [11]. It was shown that this idea in principle works in the as-fabricated [10] as well as in the embrittled material [12]. The fibres are made of W wire which was characterised in detail by means of tension tests [13–15]. Recently, a layered chemical vapour deposition process was developed allowing the production of large and reproducible samples [16]. This allowed the launch of a material characterisation program in which three point bending tests have been performed in a first step. In Charpy impact tests, it was proven that the toughening effect is still working under high deformation rates [16]. In this paper we are presenting for the first time the behavior of W_f/W under tension load as the next step in this program. Although the amount of tests was restricted to two, the results gave valuable information about the ultimate tensile strength (UTS) of W_f/W as a normalized material parameter. In addition, the detailed microstructural investigations are very helpful for the understanding and further development of W_f/W composites.

2. Materials and experimental procedure

The raw material was produced as a plate with a layered chemical vapour deposition (CVD) process performed at Archer

* Corresponding author at: Max-Planck-Institut für Plasmaphysik, 85748 Garching, Germany.
E-mail address: hanns.gietl@ipp.mpg.de (H. Gietl).

http://dx.doi.org/10.1016/j.fusengdes.2017.02.054

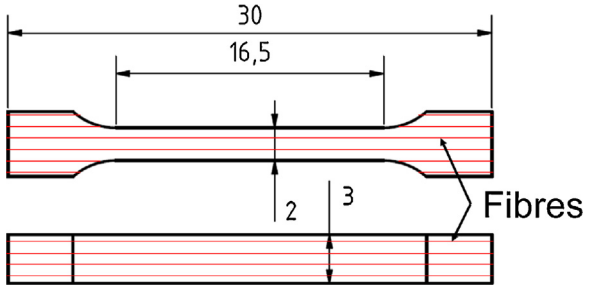

Fig. 1. Dimensions of specimen for tension tests. The (direction of) the fibres are marked in red. (For interpretation of the references to colour in this figure legend, the reader is referred to the web version of this article.)

Technicoat Ltd. (High Wycombe, UK). A detailed process description is given in [16]. Single layer of unidirectional orientated pure tungsten wires with a diameter of 150 μm were used as preforms. These preforms were coated with 1 μm thick interlayer of Er_2O_3 by magnetron sputtering according to the process description given in [17]. The successful use of Er_2O_3 as an interlayer in W_f/W has been demonstrated before [12,17,18]. The CVD process is a layer-wise process consisting of three repeating process steps. At first, the preform is placed on a heating plate inside the process chamber. Secondly, tungsten is deposited until the fibre layer is totally ingrown. Finally, the process chamber is opened to place the next preform layer on top of the already coated solid composite. This process is repeated until the aimed thickness is reached. The fibre volume ratio of the specimens is up to 30% (depending on the distance between the fibre layers) with an overall density of 94% (determined by Archimedes principle) [16]. Material consisting of 10 layers with a total thickness of approximately 3 mm was used in this experiment. Tension specimens were manufactured out of this material with electrical discharge machining (EDM), according to the geometry shown in Fig. 1. The parameters for EDM were chosen to ensure a low surface roughness, hence the specimens were not polished after EDM. The measuring length was 16.5 mm.

The tension tests were performed with a universal testing device (TIRAtest 2820, Nr. R050/01, TIRA GmbH). The load was recorded by a 20 kN load cell. A specially designed holding system was used to avoid stress peaks at the contact surface of the holder and the specimen. Moreover, the holders were mounted with a chain system to the grip of the testing device to ensure self alignment and thus an uniaxial stress-state within the specimen (Fig. 2).

Each specimen was preloaded with 20 N. The test was conducted at room temperature and displacement controlled with a constant

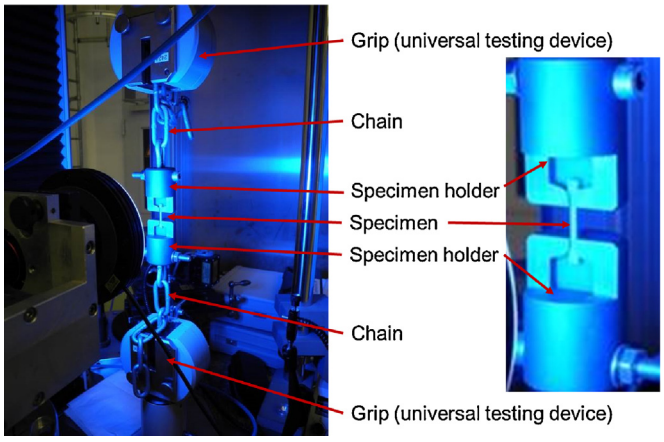

Fig. 2. Experimental setup for tension tests.

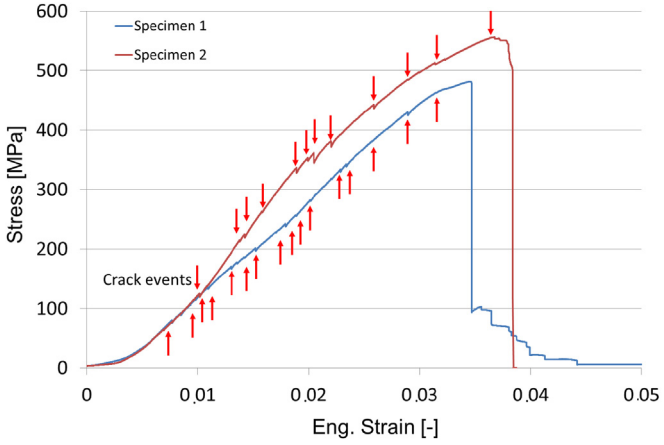

Fig. 3. Stress–strain curves for the specimens 1 and 2.

displacement rate of 10 μm/s. The strain was calculated with the corrected cross-head displacement and the individual surface area of each specimen was used to determine the stress.

Afterwards, the fractured surfaces and polished cross sections were investigated by scanning electron microscopy (SEM), confocal laser scanning microscopy (CLSM) and optical microscopy. The different viewing points on specimen 1 are shown in Fig. A1 in the appendix. In total, two samples were tested (specimen 1 and 2).

3. Results

The stress–strain curves of the two tests are shown in Fig. 3. Both stress–strain curves show a very similar behavior. At the beginning, they show a nonlinear behavior due to the setting of the system before the load is fully transferred into the specimen. After linear loading, a first load drop is detected at 80 MPa for specimen 1 and 125 MPa for specimen 2. In total 19 load drops are observed for specimen 1 and 12 load drops for specimen 2, respectively. Each load drop was accompanied with an audible cracking noise. In addition, the crack propagation was observed optically for specimen 2 at which every cracking noise was followed by the appearance of a new crack. Beside these events, the load is rising with ongoing displacement indication a rising load bearing capacity. After reaching the ultimate tensile strength (UTS) a large load drop (slightly delayed in specimen 2) accompanied by a huge crack growth is detected. Specimen 1 can still bear some load whereas specimen 2 is fully fractured. The UTS is 482 MPa (specimen 1) and 557 MPa (specimen 2) respectively.

The fracture surface of specimen 1 is shown in Fig. 4. The fibre layer which was grown first during manufacturing is on the left side of Fig. 4(a). 77 fibres are located in the sample leading to a fibre volume fraction of 22%. The fracture surface has four steps which can be seen in Fig. 4(a) and in the side view (shown in Fig. 5). The first step includes six fibre layers and has the largest area. The second and third step consist of one fibre layer each and the fourth step contains two fibre layers. The height difference from step one to two is 1.23 mm, from step two to three 0.81 mm and from step three to four 5.14 mm. The height of the steps is correlated to the layer (deposition) thickness. In step one, very few pores can be seen and these pores are distributed over the whole area. The pores are located between the deposition layers and have the typical shape caused by premature blocking of gas transport (more details in discussion). The porosity in this area is 2.2% (density: 97.8%). Large pores are located between step three and four which lead to a delamination. The fracture surface of specimen 2 had two steps with a height difference of 1.92 mm which represents the thickness of the layers and 80 fibres are located in the sample leading to

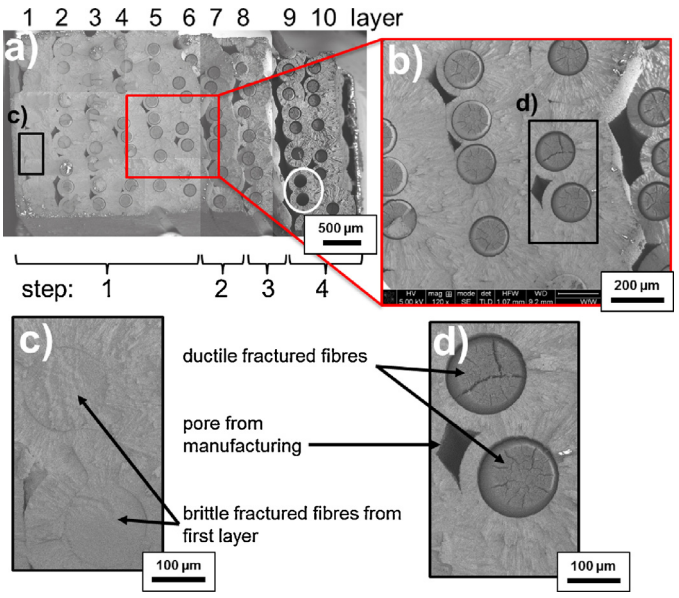

Fig. 4. SEM image of the fracture surface specimen 1. The localization is shown in Fig. A1 in the appendix.

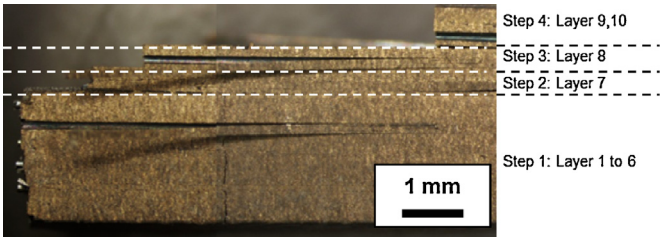

Fig. 5. Side view of the ruptured specimen 1. The localization is shown in Fig. A1 in the appendix.

Table 1
Number of fibres in the specimens.

Fibres	Total	Ductile	Brittle
Specimen 1	77	61	16
Specimen 2	80	70	10

fibre volume fraction of 21%. The first step consists of two fibre layer and within this layer no large pores are visible. However, between layer one and layer two pores with an elongated shape are located. The second step which consists of eight fibre layers has also no large pores and the porosity is below 1.9% (density: 98.1%).

Approximately 80% of the fibres of specimen 1 and over 94% of specimen 2 show a ductile behavior (Fig. 4(d)) and the rest failed in a brittle manner (Fig. 4(c)). The ductile fibres show the typically so called knife-edge fracture whereas the brittle fibres show transcrystalline cleavage or grain boundary failure [19,20]. Most of the brittle fibres were located in the first layer for both specimens (see Fig. 4(a) and (c)). Furthermore, the interlayer does not show any debonding for the brittle fibres (Fig. 4(c) while a clear debonding can be seen for the ductile fibres (Fig. 4(d)). In Table 1, the total amount of fibres as well as the number of fibres which show ductile and brittle behavior are presented for both specimens.

The second half of the ruptured specimen 1 is shown in Fig. 6. In Fig. 6(a) two cracks (indicated with red arrows) can be seen beside the already discussed steps. A total amount of 19 matrix cracks for specimen 1 and 12 matrix cracks for specimen 2 which were counted at the ruptured specimen. Two fibres which stick out of the composite indicates a massive fibre pull-out (indicated with white arrows in Fig. 6(a)). The corresponding site of the pull-out can be seen in Fig. 4(a) and is marked with a white circle.

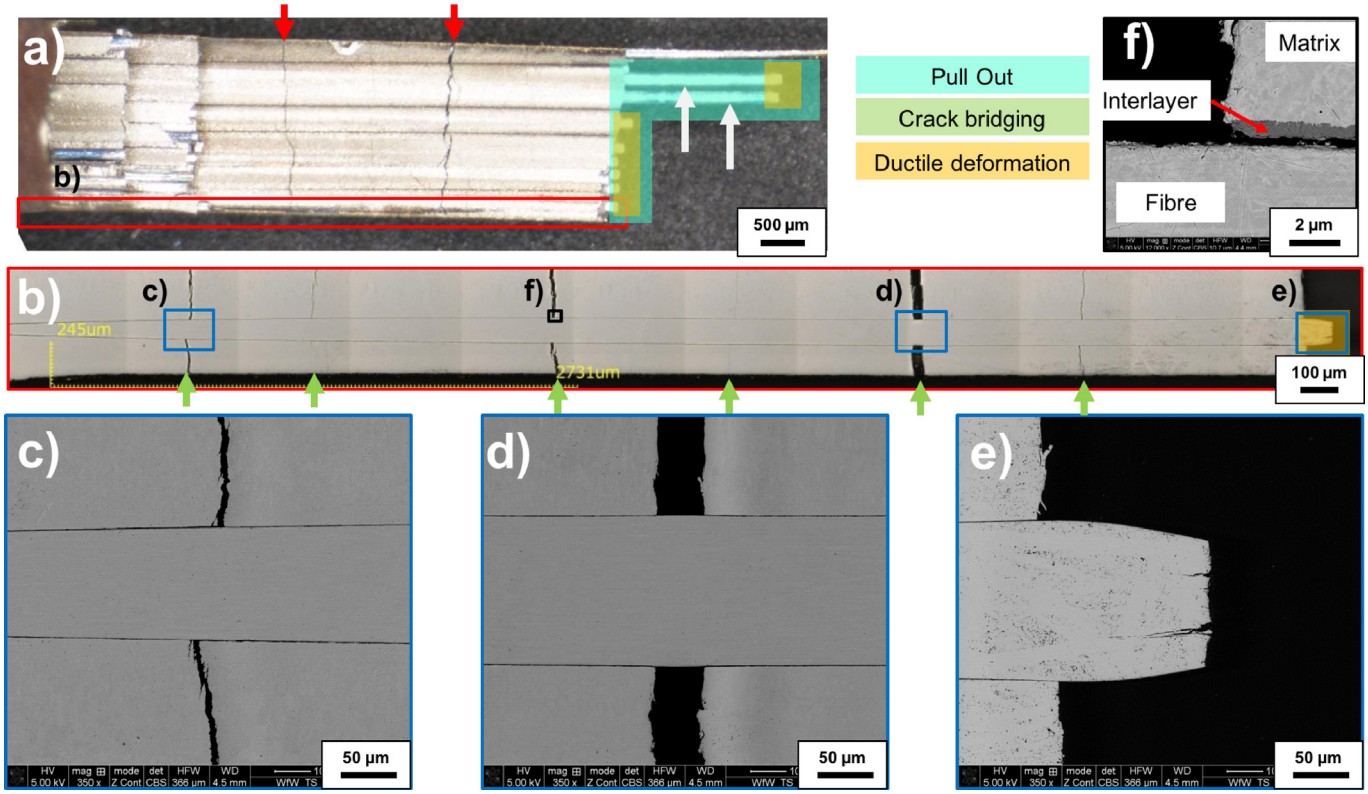

Fig. 6. Detailed view specimen 1 (a) optical microscope image, (b) CLSM image, (c)–(f) SEM images. The localization is shown in Fig. A1 in the appendix. (For interpretation of the references to colour in the text, the reader is referred to the web version of this article.)

The specimen was polished in a way that one fibre of layer 10 was cut in half. A slight off axis-angle during polishing lead to a variation in the fibre diameter visible in Fig. 6(c). Fig. 6(b) shows the detailed cross section of that fibre. The matrix is cracked six times over the shown fibre length (indicated with green arrows). These cracks are evenly distributed and show different openings. The largest crack has a width of 45 μm (Fig. 6d)). Only at the fracture surface (Fig. 6e)), the fibre shows a ductile deformation.

Fig. 6(f) shows a detailed view of a crack region where the interlayer, the fibre and the matrix are visible. The debonding is detected between interlayer and fibre whereas the bonding between interlayer and matrix is intact.

4. Discussion

As it was shown in the fracture surfaces of the specimens different steps during failure are observed. These fracture steps occurred between two different deposition layers and are most probably caused by a weak bonding between the layers. Two reasons for that can be identified. The layered deposition process faces the problem that the deposition chamber needs to be opened for placing the next fibre layer. This can lead to an oxidation or the entry of impurities leading to a weak bonding. In addition, the pores concentrated between the layers weaken the bonding. The reasons for these pores can be identified in the fibre arrangement. For the chemical deposition of W the process gas needs to access all points until a deposition of dense material is reached. Inaccuracies in the fibre arrangement can lead to premature blocking of the gas path and therefore unfilled areas which form pores. More details are given in [21,22]. The pores can lead to a stress concentration in the surrounding material and therefore weaken the composite. This can lead to a delimitation within the composite leading to the stepwise cracking. This can clearly be seen in e.g. between layer 3 and 4 of sample 1 (see Fig. 4(d)).

The cracking noise at each load drop indicates crack propagation at these events. Moreover, the number of load drops in the stress strain curves corresponds to the number of matrix cracks seen in the fractured specimens. This and the direct observation (for specimen 2) indicates that the load drops and matrix cracks are directly related. At each drop, a matrix crack is formed. However, the specimens can bear a rising load. This is a typical behavior for extrinsic toughening [23]. It is likely that the debonded fibres are load bearing and bridging the crack. This is supported by the observation shown in Fig. 6 where the bridging is shown for one fibre. Assuming that only debonded fibres survive crack initiation in the matrix, only these fibres are contributing to the ultimate strength. A theoretical UTS for a single fibre can be calculated as follows.

$$\sigma_{\text{fibre}} = F_{W_f/W} / A_{\text{all ductile fibres}}$$

This leads to theoretical fibre strength of 2680 MPa for specimen 1 and 2700 MPa for specimen 2. These values are very close to the value obtained by [13] in single fibre tension tests and therefore support our assumption that only the fibres are load bearing and that the UTS is dominated by the fibres. However, the first layer of both specimen show a brittle fracture of the fibres. This is potentially correlated to some carbon contamination. In order to remove the W_f/W plate after the production, carbon was sprayed on the heating table in the deposition chamber. As carbon diffuses into tungsten at a rather low temperatures [24,25] and can lead to an embrittlement of tungsten fibres [26], this could be a possible explanation for the presence of brittle fibres.

Specimen 1 is able to withstand 100 MPa after a massive load drop before full failure. A reason for that might be the massive pull out observed for two fibres. Although this was only observed for two fibres and such a long pull-out length will probably not be reached in a real structure, it shows the potential of pull-out effects.

Multiple matrix cracking is observed with comparable crack spacings. This was expected for W_f/W [27] and is also well known for brittle matrix composites, where the matrix has a lower failure strain than the fibre [28,29]. If the stress in the matrix reaches the critical value, the matrix breaks and the fibres bear the load while at this state the matrix has no stress. Then the stress in the matrix rises again and the next crack appears to reduce the stress in the matrix. This happens as long as the fibres are able to bear the load. This is correlated to a good fibre bonding, however with the possibility of debonding [30,31]. If the fibre and matrix do not debond, the fibres would fail together with the matrix and the material would fail like a brittle material. On the other hand, if the interlayer bonding is too weak the stress cannot be transferred from the matrix to the fibre and multiple matrix cracking would not emerge. Furthermore, no multiple necking i.a. plastic deformation for a single fibre has been observed. A possible reason is that the bonding between the fibre and matrix is not strong enough to reach the yield point of the fibres in multiple locations. This could be overcome by an enhanced (interlayer) bonding. These results show the strong dependence of the material properties on the bonding between fibre and matrix and thus on the chosen interlayer.

5. Conclusion and outlook

For the first time, pseudo ductile behavior was demonstrated for bulk W_f/W under tensile test conditions. The stress–strain diagrams of the tensile tests correspond to the curves which are well known from literature for pseudo ductile behavior of composite materials. Furthermore, the UTS was determined and multiple matrix cracking could be demonstrated for the first time in W_f/W. Moreover, most of the fibres survive the multiple matrix cracks and finally fracture in a ductile way.

It is planned to produce and test more W_f/W bulk samples with an optical strain measurement system to gather a better statistic. In addition, an optimized manufacture routine for producing the tungsten matrix is under development to improve interlayer bonding and avoid porosity. Moreover, pull-out and single fibre fragmentation tests are under preparation to investigate the bonding between fibre and matrix in more detail.

Acknowledgements

The authors want to acknowledge the Osram GmbH, Schwabmünchen, Germany for providing the tungsten wire and Archer Technicoat Ltd, High Wycombe, UK for assistance in the CVD production. This work has been carried out within the framework of the EUROfusion Consortium and has received funding from the Euratom research and training programme 2014–2018 under grant agreement No 633053. The views and opinions expressed herein do not necessarily reflect those of the European Commission.

Appendix

For the localization of the different figures (Fig. 4–6) an overview for the line of sight is shown in.

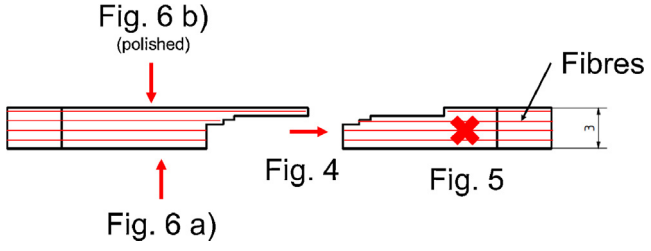

Fig. A1. Schematic sketch for the different views on specimen 1.

References

[1] J.W. Coenen, S. Antusch, M. Aumann, W. Biel, J. Du, J. Engels, S. Heuer, A. Houben, T. Höschen, B. Jasper, F. Koch, J. Linke, A. Litnovsky, Y. Mao, R. Neu, G. Pintsuk, J. Riesch, M. Rasinski, J. Reiser, M. Rieth, A. Terra, B. Unterberg, Th. Weber, T. Wegener, J.-H. You, Ch. Linsmeier, Materials for DEMO and reactor applications boundary conditions and new concepts, Phys. Scr. T167 (2016) 014002.

[2] C. Gandhi, M.F. Ashby, Overview no. 5: Fracture-mechanism maps for materials which cleave: F.C.C., B.C.C. and H.C.P. metals and ceramics., Acta Metall. 27 (10) (1979) 1565–1602.

[3] E. Lassner, W.-D. Schubert, Tungsten – Properties, Chemistry, Technology of the Element, Alloys, and Chemical Compound, Springer, 1999.

[4] J. Reiser, M. Rieth, B. Dafferner, A. Hoffmann, Charpy impact properties of pure tungsten plate material in as-received and recrystallized condition, J. Nucl. Mater. 442 (2013) 204–207.

[5] W. Yih, C. Wang, Tungsten: Sources, Metallurgy, Properties, and Applications, Springer US, 1979.

[6] V. Barabash, G. Federici, M. Rödig, L. Snead, C. Wu, Neutron irradiation effects on plasma facing materials, J. Nucl. Mater. 283–287 (2000) 138–146.

[7] J.M. Steichen, Tensile properties of neutron irradiated TZM and tungsten, J. Nucl. Mater. 60 (1976) 13–19.

[8] J. Du, T. Höschen, M. Rasinski, S. Wurster, W. Grosinger, J.-H. You, Feasibility study of a tungsten wire-reinforced tungsten matrix composite with ZrO_x interfacial coatings, Compos. Sci. Technol. 70 (2010) 1482–1489.

[9] J. Du, T. Höschen, M. Rasinski, J.-H. You, Shear debonding behavior of a carbon-coated interface in a tungsten fiber-reinforced tungsten matrix composite, J. Nucl. Mater. 417 (2011) 472–476.

[10] J. Riesch, T. Höschen, Ch. Linsmeier, S. Wurster, J.-H. You, Enhanced toughness and stable crack propagation in a novel tungsten fibre-reinforced tungsten composite produced by chemical vapour infiltration, Phys. Scr. T159 (2014) 014031.

[11] A.G. Evans, Perspective on the development of high-toughness ceramics, J. Am. Chem. Soc. 73 (1990) 187–206.

[12] R. Neu, J. Riesch, J.W. Coenen, J. Brinkmann, A. Calvo, S. Elgeti, C. Garcia-Rosales, H. Greuner, T. Höschen, G. Holzner, F. Klein, F. Koch, Ch. Linsmeier, A. Litnovsky, T. Wegener, S. Wurster, J.-H. You, Advanced tungsten materials for plasma-facing components of DEMO and fusion power plants, Fusion Eng. Des. 109–111 (Part A) (2016) 1046–1052.

[13] P. Zhao, J. Riesch, T. Höschen, J. Almannstötter, M. Balden, J.W. Coenen, U. Himml, U. von Toussaint, R. Neu, Microstructure, mechanical behavior and fracture of pure tungsten wires after different heat treatments, Int. J. Refract. Met. Hard Mater. (2016) (in preparation).

[14] J. Riesch, J. Almannstötter, J.W. Coenen, M. Fuhr, H. Gietl, Y. Han, T. Höschen, Ch. Linsmeier, N. Travitzky, P. Zhao, Properties of drawn w wire used as high performance fibre in tungsten fibre-reinforced tungsten composite, IOP Conf. Ser. Mater. Sci. Eng. 136 (2016) 012043.

[15] J. Riesch, Y. Han, J. Almannstötter, J.W. Coenen, T. Höschen, B. Jasper, P. Zhao, Ch. Linsmeier, R. Neu, Development of tungsten fibre-reinforced tungsten composites towards their use in DEMO – potassium doped tungsten wire, Phys. Scr. T167 (2016) 014006.

[16] J. Riesch, M. Aumann, J.W. Coenen, H. Gietl, G. Holzner, T. Höschen, P. Huber, M. Li, Ch. Linsmeier, R. Neu, Chemically deposited tungsten fibre-reinforced tungsten – the way to a mock-up for divertor applications., Nucl. Mater. Energy 9 (2016) 75–83.

[17] J. Du, A feasibility study of tungsten-fiber-reinforced tungsten composites with engineered interfaces (PhD thesis), Technische Universität München, 2010.

[18] R. Neu, J. Riesch, A.v. Müller, M. Balden, J.W. Coenen, H. Gietl, T. Höschen, M. Li, S. Wurster, J.-H. You, Tungsten fibre-reinforced composites for advanced plasma facing components, Nucl. Mater. Energy (2016), Available online 28 November 2016, (in press).

[19] S. Leber, J. Tavernelli, D.D. White, Fracture modes in tungsten wire, J. Less Common Metals 48 (1976) 119–133.

[20] P. Schade, 100 years of doped tungsten wire, Int. J. Refract. Met. Hard Mater. 28 (2010) 648–660.

[21] J. Riesch, Entwicklung und Charakterisierung eines wolframfaserverstrkten Wolfram-Verbundwerkstoffs (PhD thesis), Technische Universität München, 2012.

[22] J. Riesch, T. Höschen, A. Galatanu, J-H. You, Tungsten-fibre reinforced tungsten composites: a novel concept for improving the toughness of tungsten, in: Proceedings of the Eighteenth International Conference on Composite Materials, Jeju, South Korea, 2011.

[23] K.K. Chawla, Ceramic Matrix Composites, Springer US, 2001.

[24] J. Luthin, Ch. Linsmeier, Carbon films and carbide formation on tungsten, Surf. Sci. 454 (456) (2000) 78–82.

[25] H. Maier, M. Rasinski, E. Grigore, C. Ruset, H. Greuner, B. Böswirth, G.F. Matthews, M. Balden, S. Lindig, JET-EFDA, Performance of W coatings on CFC with respect to carbide formation, J. Nucl. Mater. 415 (2011) 310–312.

[26] A. Kelly, W.R. Tyson, Tensile properties of fibre-reinforced metals: copper/tungsten and copper/molybdenum, J. Mech. Phys. Solids 13 (1965) 329–338.

[27] J. Riesch, J.Y. Buffiere, T. Höschen, M. di Michiel, M. Scheel, Ch. Linsmeier, J.-H. You, In situ synchrotron tomography estimation of toughening effect by semi-ductile fibre reinforcement in a tungsten-fibre-reinforced tungsten composite system, Acta Mater. 61 (2013) 7060–7071.

[28] W.A. Curtin, Multiple matrix cracking in brittle matrix composites, Acta Metal. Mater. 41 (5) (1993) 1369–1377.

[29] X.F. Yang, K.M. Knowles, The one-dimensional car parking problem and its application to the distribution of spacings between matrix cracks in unidirectional fiber-reinforced brittle materials, J. Am. Ceram. Soc. 75 (1) (1992) 141–147.

[30] M.-Y. He, J.W. Hutchinson, Crack deflection at an interface between dissimilar elastic materials, Int. J. Solids Struct. 25 (1989) 1053–1067.

[31] A.G. Evans, F.W. Zok, J. Davis, The role of interfaces in fiber-reinforced brittle matrix composites, Compos. Sci. Technol. 42 (1991) 3–24.